

Article

Damage to Buildings in Large Slope Rock Instabilities Monitored with the PSInSAR™ Technique

Paolo Frattini ^{1,*}, Giovanni B. Crosta ¹ and Jacopo Allievi ²

¹ Department of Earth and Environmental Sciences, Università degli Studi di Milano-Bicocca, p.zza della Scienza 4, 20126 Milan, Italy; E-Mail: giovannibattista.crosta@unimib.it

² Tele-Rilevamento Europa T.R.E., Ripa di Porta Ticinese 79, 20143 Milan, Italy; E-Mail: jacopo.allievi@treuropa.com

* Author to whom correspondence should be addressed; E-Mail: paolo.frattini@unimib.it; Tel.: +39-02-6448-2005; Fax: +39-02-6448-2073.

Received: 30 July 2013; in revised form: 17 September 2013 / Accepted: 17 September 2013 / Published: 25 September 2013

Abstract: The slow movement of active deep-seated slope gravitational deformations (DSGSDs) and deep-seated rockslides can cause damage to structures and infrastructures. We use Permanent Scatterers Synthetic Aperture Radar Interferometry (PSInSAR™) displacement rate data for the analysis of DSGSD/rockslide activity and kinematics and for the analysis of damage to buildings. We surveyed the degree of damage to buildings directly in the field, and we tried to correlate it with the superficial displacement rate obtained by the PSInSAR™ technique at seven sites. Overall, we observe that the degree of damage increases with increasing displacement rate, but this trend shows a large dispersion that can be due to different causes, including: the uncertainty in the attribution of the degree of damage for buildings presenting wall coatings; the complexity of the deformation for large phenomena with different materials and subjected to differential behavior within the displaced mass; the absence of differential superficial movements in buildings, due to the large size of the investigated phenomena; and the different types of buildings and their position along the slope or relative to landslide portions.

Keywords: deep-seated slope deformation; rock slide; PSInSAR™ displacements; damage; buildings

1. Introduction

Large slow-moving non-catastrophic slope rock instabilities represent an important geological risk. They can cause the deformation of structures and infrastructures (*i.e.*, dams, tunnels, railway tracks, buildings, [1–3]) and, due to the damage of rock masses, resulting in the decay of mechanical properties, secondary landslides can be triggered within their limits [1]. Large slope rock instabilities include both very large rockslides and deep-seated gravitational slope deformations (DSGSDs) [4,5], the latter being characterized by the involvement of entire valley flanks, the presence of gravitational morphostructures (e.g., large scarps, open or infilled trenches, downthrown blocks, ridge top depressions, grabens, double or multiple ridges and counterscarps) and the geomorphological evidence of slope deformation and displacements along individual structures and inherited tectonic features [1,6–10]. Although DSGSD has been considered until recently to be a class of relict phenomena inactive under present climatic conditions, geomorphological and geochronological evidence recently demonstrated that movements associated with large slides and DSGSD, although slow, can continue for long periods, producing large cumulative displacements [11–14]. Reactivation may also happen after long periods of quiescence or inactivity. Surface displacements typically range from a few millimeters to several centimeters per year and are commonly close to the detection precision of monitoring equipment [8,15].

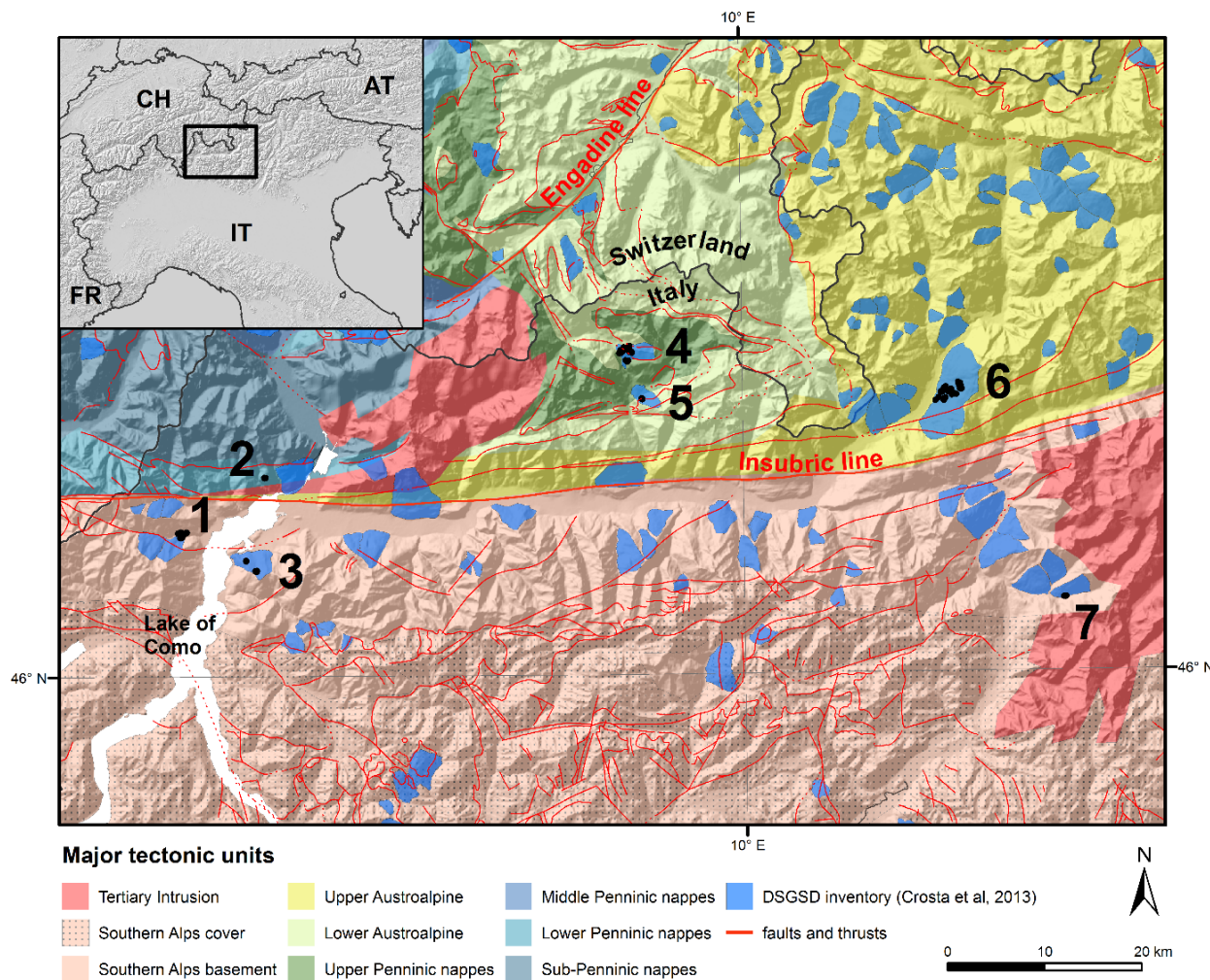
Recently, SAR (Synthetic Aperture Radar) interferometry [16–20] has been demonstrated to be a suitable technique to monitor these movements [1,21–31]. [21,22] used the Permanent Scatterers technique (PSInSAR™, [20]) to study DSGSDs (*i.e.*, Varadega or Confinale-Cima di Saline), landslides (*i.e.*, Ruinon) and active scree slope (*i.e.*, Premadio area) in the Central Italian Alps. [1] studied some DSGSDs from a structural point of view by using PSInSAR™ datasets; they described six different DSGSDs (*i.e.*, Mt. Varadega, Mt. Resverde, Mt. Pesciola, Mt. Baita Meriggio, Mt. Legnoncino and Mt. Cortafò) to demonstrate that the PSInSAR™ technique could give significant results in DSGSD detection and monitoring. Besides satellite-based SAR interferometry, ground-based SAR has been also applied to the investigation and monitoring of Alpine rockslides [32]. Damage to structures and infrastructures induced by very slow-moving rockslides has been rarely investigated [33–36], with special focus on infrastructures that have experienced significant deformation [1–3].

In this paper, we analyze seven DSGSDs and rockslides located in the Central Italian Alps (Lombardy Region, Northern Italy). These landslides are extracted from DSGSD and large landside inventories recently created for the entire Alpine range [5,37–39]. The aim of the paper is to analyze large slope movements in conjunction with radar interferometry and damage data in order to investigate the state of the activity of such phenomena and to describe the resulting level of damage as a function of the ground surface rate of movement.

2. Geological and Geomorphologic Setting

The study area lies in the Alpine sector of the Lombardy Region (northern Italy) (Figure 1), which is composed of three main structural units [40–43]: Southern Alps, the Penninic unit and the Austroalpine domain.

Figure 1. Location of the studied deep-seated gravitational slope deformations (DSGSDs) and rockslides: (1) Catasco rockslide; (2) Montalto rockslide; (3) Mt. Legnoncino DSGSD; (4) Lake Palù DSGSD; (5) Caspoggio DSGSD; (6) Mt Padrio-Varadega DSGSD; (7) Savio DSGSD. Mapped major tectonic units and structures modified from [40,43], respectively. DSGSD polygons are from [5]. Black dots refer to surveyed buildings. CH: Switzerland; AT: Austria; FR: France; IT: Italy.



These units are separated by the Insubric line, representing a steeply north dipping and east-west trending fault zone. The Southern Alps represent the most recent part, interpreted as a fold-and-thrust system, where rocks can be divided into basement and sedimentary cover [41].

The units to the north of the Insubric line consist of the Austroalpine nappes to the east and the Penninic nappes to the west. Austroalpine units, although of similar paleogeographic provenance as the Southern Alps, consist of a completely rootless metamorphic basement and sedimentary cover that were detached from their lithosphere as early as the Cretaceous orogenesis [42]. The Penninic units are of extremely heterogeneous paleogeographic provenance, including remnants of oceanic lithosphere (Malenco-Forno unit), as well as basement of the European margin (Adula, Tambò and Suretta units).

The Alpine territory is characterized by high mountains and deep valleys producing high relief energy. This morphology results from the combined action of geological structure, climate and its changes, causing a different action by glaciations and the fluvial system.

Seven slow-moving large slope instabilities have been analyzed in this paper (Figure 1). The Catasco rockslide (#1 in Figure 1), Mt. Legnoncino DSGSD (#3 in Figure 1) and Saviore DSGSD (#7 in Figure 1) occur in the basement of the Southern Alpine nappe. The lithology of these different sites is quite similar, mainly consisting of paragneiss and schist. The Montalto rockslide (#2 in Figure 1) belongs to the lower Penninic nappe, and its lithology is characterized by paragneiss. The Lake Palù DSGSD (#4 in Figure 1) and Caspoggio DSGSD (#5 in Figure 1) lie at the contact between the Upper Penninic nappe and the Austroalpine basement. Here, the Penninic units are composed of oceanic ophiolites and serpentines and the Austroalpine units of gneiss and schists. The Mt. Padrio-Varadega DSGSD (#6 in Figure 1) belongs to the Austroalpine basement, and the lithology consists of gneiss (Punta della Pietra Rossa Formation).

3. Material and Methods

3.1. PSInSAR™

PSInSAR™, Permanent Scatterers Synthetic Aperture Radar Interferometry, is an advanced interferometric technique developed at the end of 1990 by the SAR group of Milan Politecnico and T.R.E. (Tele-Rilevamento Europa) [17–20]. It is based on the processing of a long series of radar data acquired in the same geometry over the same area in order to single out those pixels, referred to as Permanent or Persistent Scatterers (PS), which have a “constant” electromagnetic behavior in all the radar images. This concept has been successively adopted by other researchers with similar PS processing tools [44–47]. If the scatterers correspond to objects whose reflectivity does not vary through time, temporal decorrelation is negligible and the average displacement rate can be determined with millimetric precision, removing the typical artefacts and noising affecting the traditional interferometric analysis (InSAR) [17–20,25]. The availability of long radar image archives, covering almost two decades, allows for obtaining ground displacement data since 1992, which is often not possible with more traditional methods, such as levelling and GPS surveys. PSInSAR™ displacements are measured along the satellite line of sight (LOS), which is the sensor to target direction, tilted at a θ angle to the vertical. Average displacement rate values can be both positive and negative. In the first case, the target approaches the sensor; in the second case, it moves away from the sensor. Due to the acquisition satellite geometry (the sensor flies along an orbit with an approximately N-S direction, acquiring a line of sight orthogonal to the orbit), InSAR measurements are not capable of detecting movements in the same N-S direction of the orbit. The combination between satellite orbit and Earth rotation allows the sensor to acquire data in two modes (Figure 2). The reference points are selected based on a statistical procedure that minimizes the standard deviation of measurements [48]. Later, the points are checked to verify if they are reliable stable points from a geological point of view.

Different satellites detect points at regular time intervals (revisiting time): European Remote-Sensing satellites 1 and 2 (ERS1 and ERS2) every 35 days and Radarsat-1 (RSAT-S3) every 24 days. For our analysis, we used different datasets with ERS (1/2) and RSAT-S3 data (Tables 1 and 2 and Supplementary Material) and processed using the Standard PS Analysis (SPSA) processing engine [20].

LOS displacement data for each dataset have been converted to the direction of the maximum slope, assuming that the deformation is translational and parallel to the slope [25,49,50]. Although this assumption is not straightforward, we believe that the displacement vector along the slope improves

the interpretation of deformation with respect to building damage. The precision (in terms of standard deviation) of PSInSAR™ displacements has been calculated at each site by averaging, within the instability area, the standard deviation of each single measurement (Table 2).

Figure 2. Satellite acquisition geometry: look direction and angle between the azimuth and north direction, δ , for (a) ascending and (b) descending modes; (c) local incidence angle, θ .

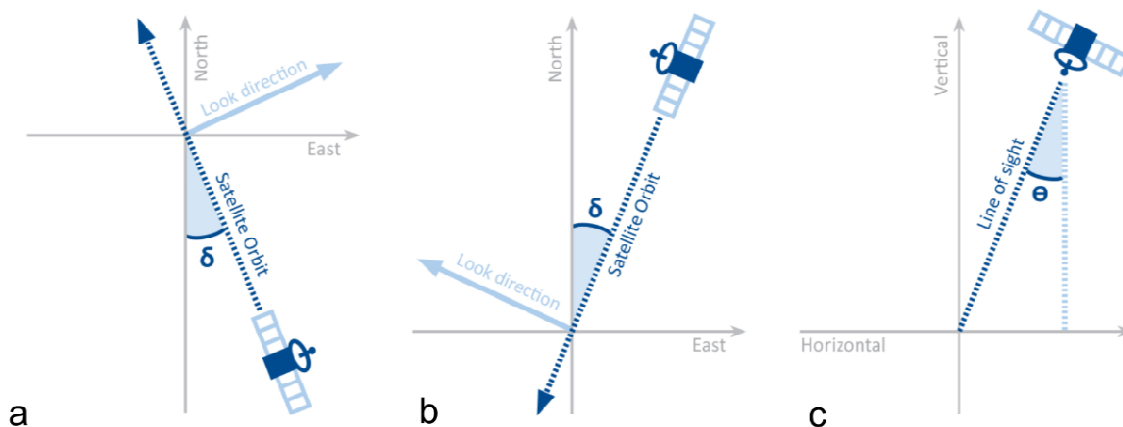


Table 1. Synthetic Aperture Radar (SAR) datasets used for the analyses. D = descending; A= ascending; θ = local incidence angle of the center of the area of interest; δ = angle between the azimuth and north direction.

Dataset Name	Satellite	Mode	Track	θ (°)	δ (°)	# of Scenes	Time Interval
LcED	ERS 1/2	D	208	23.09	11.99	80	05/16/1992–12/24/2002
			480	23.11	12.50	82	04/30/1992–01/12/2003
LED	ERS 1/2	D	208	23.09	11.99	81	05/16/1992–12/19/2000
			197	32.50	10.46	56	04/28/2003–06/18/2007
LRD	RSAT-S3	D	297	35.78	9.60	56	04/11/2003–06/01/2007
			147	34.49	11.51	59	03/07/2003–06/14/2007
LRA	RSAT-S3	A	247	32.60	12.15	59	04/07/2003–06/21/2007

Table 2. Slope geometry and information about the SAR datasets available at each site. $\bar{\beta}$ = average slope gradient; $\bar{\alpha}$ = modal slope aspect; $\bar{\sigma}$ = average standard deviation of Permanent Scatterers Synthetic Aperture Radar Interferometry (PSInSAR™) displacement rates. Numbers are as in Figure 1.

#	Site	$\bar{\beta}$ (°)	$\bar{\alpha}$ (°)	Dataset Name	# Points	$\bar{\sigma}$ (mm/yr)
1	Catasco rockslide	29	184	LRA	226	0.95
				LRD	193	0.93
2	Montalto rockslide	28	190	LRA	19	0.96
				LRD	17	0.95
				LcED	1,050	0.90
3	Mt. Legnoncino DSGSD	29	340	LRA	159	0.96
				LRD	345	0.94
				LED	269	0.62
4	Lake Palù DSGSD	18	262	LRA	143	0.96
				LRD	319	0.95

Table 2. Cont.

#	Site	$\bar{\beta}$ (°)	$\bar{\alpha}$ (°)	Dataset Name	# Points	$\bar{\sigma}$ (mm/yr)
5	Caspoggio DSGSD	26	312	LED	514	0.58
				LRA	859	1.06
				LRD	786	0.94
6	Mt. Padrio-Varadega DSGSD	28	290	LED	648	0.56
				LRA	172	1.34
				LRD	1,948	1.17
7	Saviore DSGSD	175	25	LRA	349	1.37
				LRD	623	1.17

3.2. Damage Survey

A field survey was performed to map the degree of damage of 182 buildings located on the studied sites. The surveyed buildings have been selected based on the distribution of PSInSAR™ points, to be sure that a reliable value of the displacement rate was available for each of them. For each building, we collected the GPS location and a photographic documentation of surveyed damages. If possible, interviews with local people have been conducted to reconstruct the damage history of the buildings.

Table 3. Building damage classification scheme, modified from [51]. Half-class values (e.g., 2.5) are also used to discriminate damage levels intermediate between two classes.

Degree of Damage	Description of Damage to Structures
0 None	No damage.
1 Negligible to slight	Hairline cracks in a few walls, falling of small pieces of plaster only. Falling of loose stone from the upper parts of buildings in very few cases.
2 Moderate	Cracks in many walls. Falling of large pieces of plaster. Partial collapse of chimneys.
3 Substantial to heavy	Large and extensive cracks in most of the walls. Roof tiles detached. Chimney fracture at the roofline; failure of individual non-structural elements.
4 Very heavy	Serious failure of walls; partial structural failure of roof and floors.
5 Destruction	Total or near total collapse.

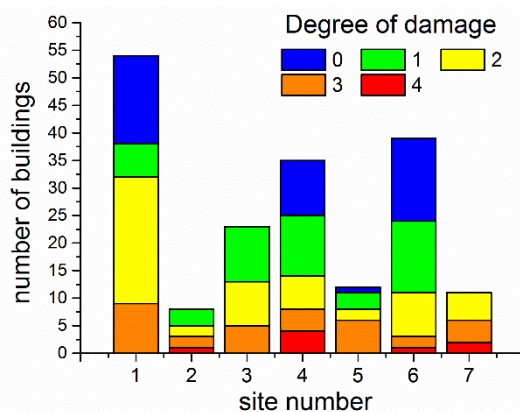
Figure 3. Examples of photographic documentation of damage reclassified according to the adopted classification (see Table 3).



For classification of the degree of damage (Table 3, Figure 3), we adopted a methodology derived from the European Macroseismic Scale [51]. For buildings showing damage intermediate between two

classes, we assigned a half-class value (e.g., 2.5). Among the surveyed buildings, 75% are damaged (Figure 4) and about 20% of the buildings are severely damaged (damage class 3 to 4).

Figure 4. Frequency of buildings reclassified according to the proposed degree of damage scale. The original values of the degree of damage have been truncated. #1: Catasco rockslide (54 buildings), #2: Montalto rockslide (8), #3: Mt. Legnoncino DSGSD (23), #4: Lake Palù DSGSD (35), #5: Caspoggio DSGSD (12), #6: Mt. Padrio-Varadega DSGSD (39); #7: Saviole DSGSD (11).



4. Analysis and Results

To understand the relationship between damage and the type and geometry of the instability, we prepared for each site a map displaying the available PSInSAR™ data, the surveyed buildings and the extent of the slope instability phenomenon. Moreover, we prepared a longitudinal swath profile of the displacement rate. To this aim, the profile along the longitudinal axis of the rock instability was subdivided into 100 m-long segments, from which polygons perpendicular to the down-slope direction and extending up to the lateral boundary of the instability have been created. By considering the PSs inside each landslide polygon, we calculated the average displacement rate and represented its trend in the plots. This approach for the construction of the displacement-rate profile was preferred with respect to the interpolation of the PSInSAR™ data, because it allows averaging over the entire width of the instability, which is an advantage where the PSInSAR™ targets are not evenly distributed within the rock instability. In the following, we present the results for each one of the sites obtained according to the above described methodology.

4.1. Mt Legnoncino

The northern flank of Mt. Legnoncino (#3 in Figure 1) is affected by a 7 km² DSGSD moving toward Como Lake (Figure 5). PSInSAR™ data show displacement rates ranging from −2 to −12 mm/yr. The displacement time series show a nearly linear trend in time, both for the upper and the lower part of the slope (Figure 6). The spatial pattern of movement is in good agreement with structural lineaments and reactivated landslides, showing a progressive downslope decrease, which suggests an increase in the horizontal component close to the DSGSD toe [1].

Figure 5. Displacement rate and damage to buildings for the Mt. Legnoncino DSGSD. (a) PSInSAR™ displacement rate map and location of the surveyed buildings (black polygons); (b) longitudinal swath profile of the displacement rate for available PS datasets; (c) damage degree of buildings as a function of the displacement rate for the LRD dataset; (d) damage degree of buildings as a function of the displacement rate for the LRA dataset. Solid and open triangles in panels (c,d) refer to buildings with and without wall coating, respectively. The grey area in panels (b,d) represents the average standard deviation (Table 2). LOS, line of sight.

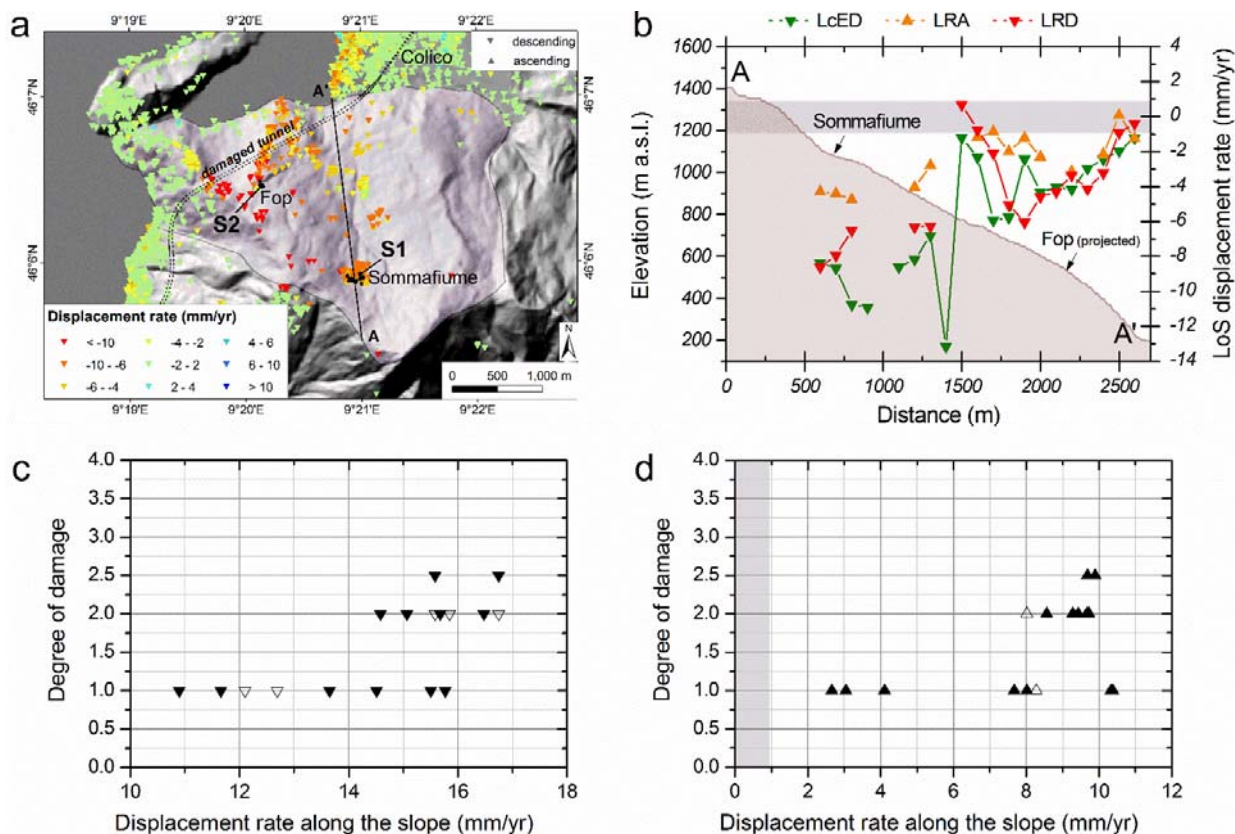
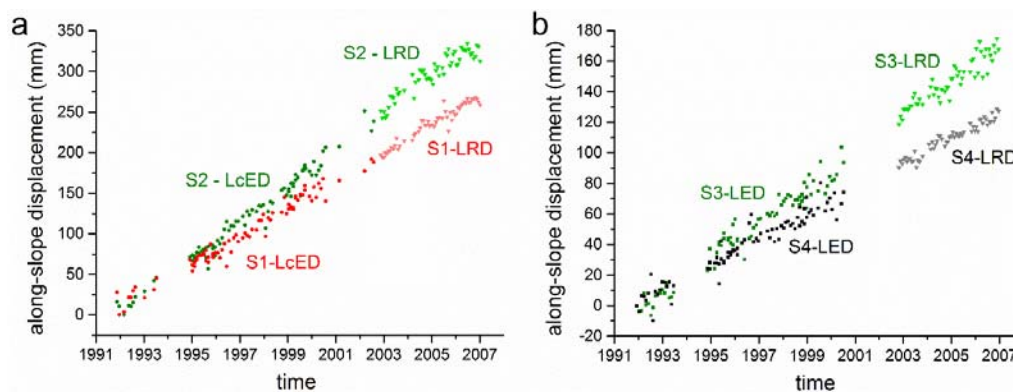


Figure 6. PSInSAR™ displacement time series for (a) Mt. Legnoncino DSGSD, sites S1 and S2 in Figure 5a, and (b) Mt. Padrio-Varadega DSGSD, sites S3 and S4 in 1st figure in Section 4.3. The displacements monitored with ERS 1-2 satellites (LcED, LED datasets) were extrapolated to 2003 and added to the LRD displacements to show a continuous time history of the sites.



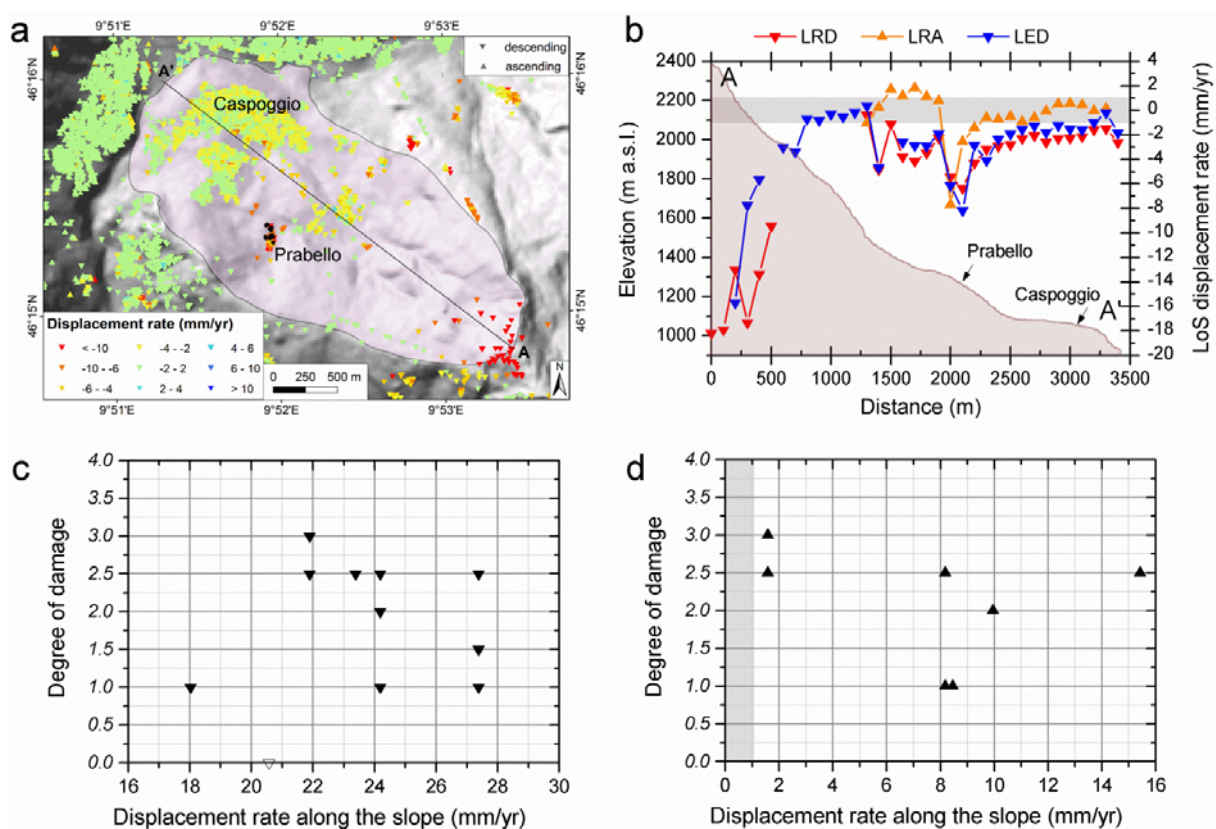
Due to the northward orientation of the slope, we can assume that PS data partially underestimate the actual movement, for the lack of capability to detect N–S-oriented movements, which are predominant in the DSGSD.

All the surveyed buildings show damages, but the degree of damage is mostly low or moderate. Both ascending and descending PSInSAR™ data seem to be correlated to the degree of damage (Figure 5c,d), as suggested by a general increasing trend of damage with displacement rate. Damages are also reported along the railway tunnel and along both tubes of the SS36 highway (Figure 5a). The latter required repairing of the tunnel concrete support because of large episodic displacements occurring in 2002 and 2012 and causing an approximate direct cost of 40 million euros. Unfortunately, these episodes are not detectable in the PSInSAR™ displacement time series, because of a lack of data during these periods (Figure 6).

4.2. Caspoggio and Lake Palù DSGSDs

Caspoggio DSGSD (Figure 7, #5) and Lake Palù DSGSD (Figure 8, #4) show a significant ground surface displacement rate, up to 20 mm/yr in magnitude along the LOS.

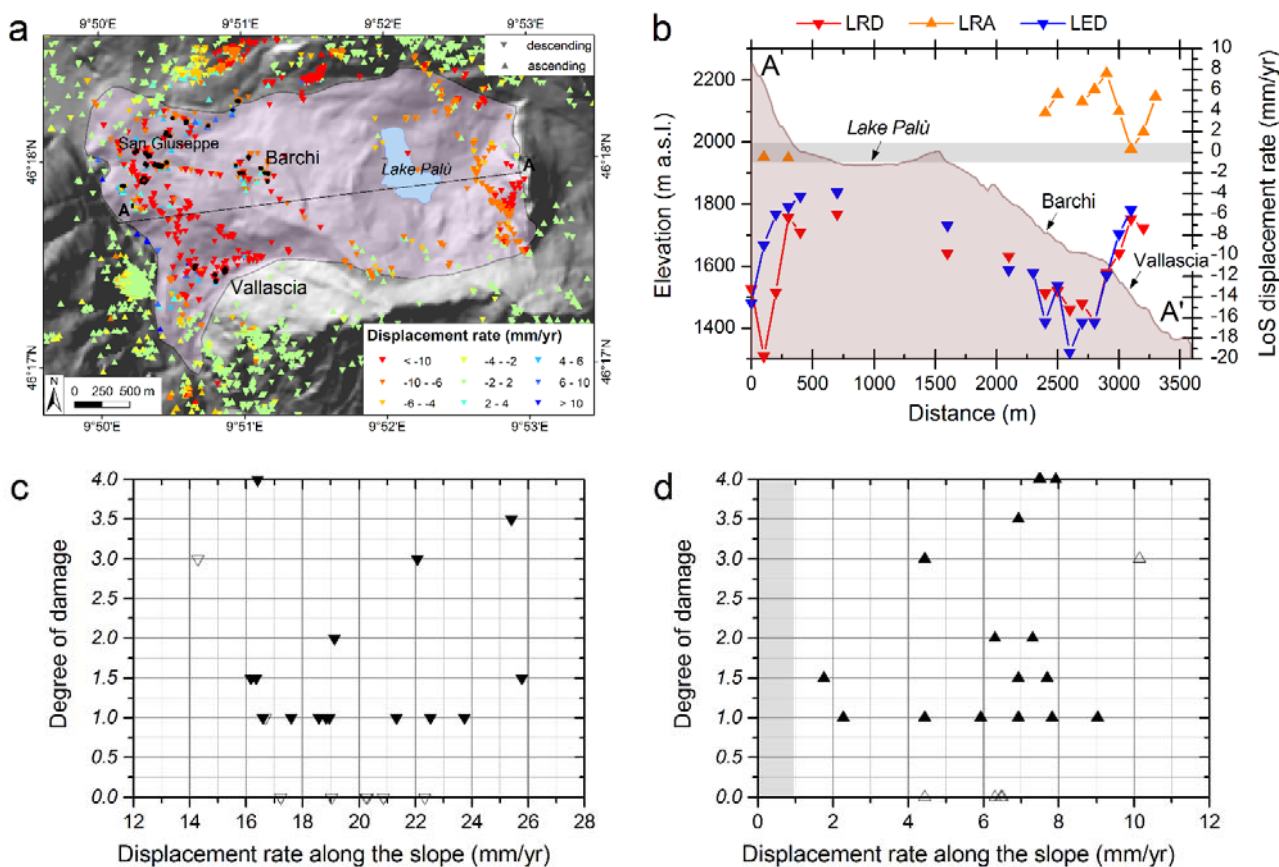
Figure 7. Displacement rate and damage to buildings for the Caspoggio DSGSD. (a) PSInSAR™ displacement rate map and location of the surveyed buildings (black polygons); (b) longitudinal swath profile of the displacement rate for available PS datasets; (c) damage degree of buildings as a function of the displacement rate for the LRD dataset; (d) damage degree of buildings as a function of the displacement rate for the LRA dataset. Solid and open triangles in panels (c,d) refer to buildings with and without wall coating, respectively. The grey area in panels (b,c) represents the average standard deviation (Table 2).



For both DSGSDs, the displacement rate is larger in the upper part of the landslide, and decreases toward the toe of the DSGSD. Again, this behavior suggests a failure mechanism with a prominent vertical downward movement in the upper part and a more horizontal movement in the lower part of the landslide. This subcircular mechanism results in positive displacement rates in the lower slope sector, where the direction of the LOS is against the slope aspect (*i.e.*, the satellite has a frontal view of the landslide). This behavior is particularly clear for the Lake Palù DSGSD (Figure 8).

For both DSGSDs, we observe significant damage to buildings. Apparently, we cannot observe a trend of increasing damage with displacement rate. Damages in the Caspoggio DSGSD have been also reported for the hydroelectric penstock and the derivation tunnel located along the northern sector of the instability [52].

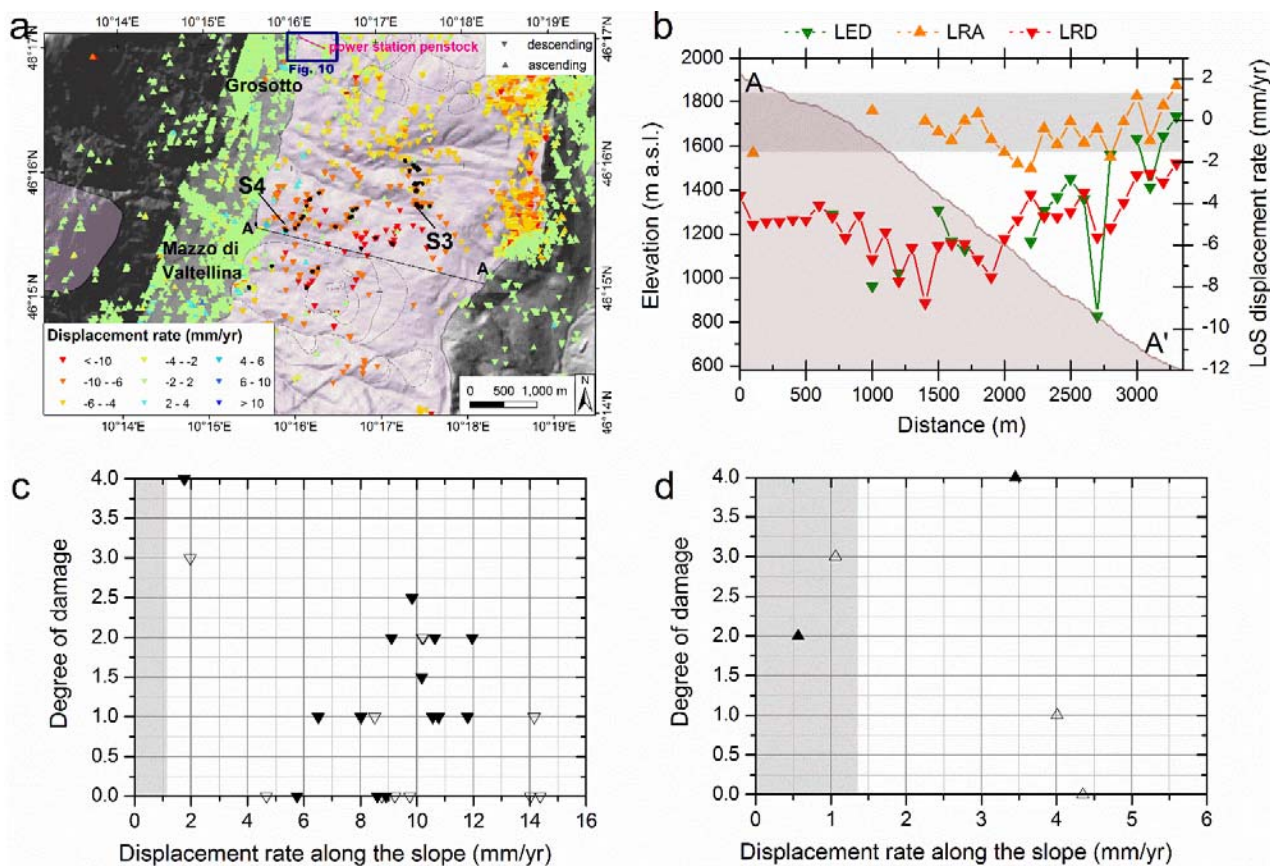
Figure 8. Displacement rate and damage to buildings for the Lake Palù DSGSD. (a) PSInSAR™ displacement rate map and location of the surveyed buildings (black polygons); (b) longitudinal swath profile of the displacement rate for available PSI datasets; (c) damage degree of buildings as a function of the displacement rate for the LRD dataset; (d) damage degree of buildings as a function of the displacement rate for the LRA dataset. Solid and open triangles in panels (c,d) refer to buildings with and without wall coating, respectively. The grey area in panels (b,d) represents the average standard deviation (Table 2).



4.3. Mt. Padrio Varadega DSGSD

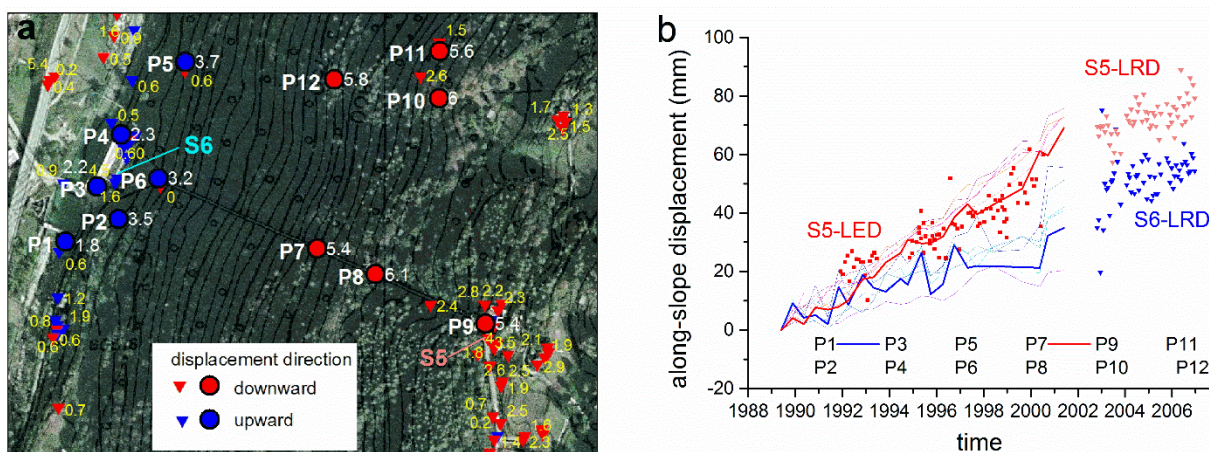
The Padrio-Varadega DSGSD (Figure 9) is a large phenomenon, with differential internal movements due to large secondary landslides [21]. Overall, a progressive decrease of LOS displacement rate can be observed moving downslope, possibly due to a sub-circular or compound failure plane [1,21]. The displacement time series show a linear behavior both for ERS 1-2 data and RSAT-S32 data (Figure 6). A good agreement is observed between geodetic and PSInSARTM measurements for the hydroelectric power plant and the penstock located in the northern sector of the DSGSD (Figure 10) [1]. This provides a long-term validation of the PSInSARTM technique, even if limited to a single sector of the DSGSD. For this study, we investigated buildings located in the central sector of the DSGSD, where the movements are also concentrated, because of the presence of secondary landslides within the main DSGSD. The ascending acquisition mode is unfavorable, due to the slope aspect, but shows a slightly positive displacement in the LOS direction, thus suggesting a sub-horizontal movement of the DSGSD toe.

Figure 9. Displacement rate and damage to buildings for the Mt. Padrio-Varadega DSGSD. (a) PSInSARTM displacement rate map and location of the surveyed buildings (black polygons); (b) longitudinal swath profile of the displacement rate for available PSI datasets; (c) damage degree of buildings as a function of the displacement rate for the LRD dataset; (d) damage degree of buildings as a function of the displacement rate for the LRA dataset. Solid and open triangles in panels (c,d) refer to buildings with and without wall coating, respectively. The grey area in panels (b,d) represents the average standard deviation (Table 2).



This movement has been also observed by geodetic measurements at the hydropower station (Figures 9 and 10, [1]) located on the alluvial deposits at the slope toe. Significant damage to residential buildings with a clear correlation with the displacement rate obtained by the descending PSInSAR™ data can be observed, with a few exceptions. In particular, the two buildings showing heavy damage and a small displacement rate in descending acquisition mode are located in the lower part of the slope, where the apparent direction of the movement becomes sub-horizontal and poorly visible in descending mode. In turn, these two buildings seem to be slightly correlated with positive displacement rates in ascending acquisition mode. The hydroelectric power plant underwent a complete stop for restoration and to allow for proper functioning of the turbines.

Figure 10. Comparison between geodetic and PSInSAR™ in the northern sector of the Mt. Padrio-Varadega DSGSD (see Figure 9a for location): (a) Displacement rate map, with geodetic monitoring (circles) and PSInSAR™ (triangles) points. The displacement rates reported in the figures are calculated along the slope direction. (b) Displacement time series for geodetic (lines) and PSInSAR™ (squares for ERS 1-2 and triangles for RSAT-S3) data. The PSInSAR™ displacements were shifted according to geodetic data to show a continuous time series.



4.4. Saviore DSGSD

Similar to Mt Padrio Varadega DSGSD, the Saviore DSGSD (Figure 11) is a complex phenomenon with secondary landslides affecting large part of the DSGSD [53]. Movements in the upper part of the slope are probably overestimated, due to the creeping of debris deposits moving faster than the DSGSD. In the southeastern sector of the DSGSD, it is possible to isolate movements associated with secondary rockslides, one of which has been recognized since the 1950s, due to damage to the Valle village. This phenomenon has been monitored since 1987 with inclinometers, optical targets and crack meters installed on the most critical buildings [53,54]. Superficial monitoring data have been obtained by [54] and compared with displacements observed by PSInSAR™ data inside the rockslide. The latter appear to underestimate the actual landslide movements, due to the impossibility to fully characterize the N-S movements, which are predominant in the rockslide (Figure 11). However, we observe a good agreement of measured satellite displacement with the E-W and vertical components of the actual displacement vector (Figure 12) measured by a total station surveying a series of optical targets.

Figure 11. Displacement rate and damage to buildings for the active rockslide inside the Saviore DSGSD. (a) PSInSAR™ displacement rate map and location of the surveyed buildings (black polygons); (b) longitudinal swath profile of the displacement rate for available PSI datasets; (c) damage degree of buildings as a function of the displacement rate for the LRA dataset; (d) damage degree as a function of the crack meter displacement rate. Solid and open triangles in panel (c) refer to buildings with and without wall coating, respectively. Open circles in panel (d) refer to cemetery wall. The grey area in panel (b) represents the average standard deviation (Table 2).

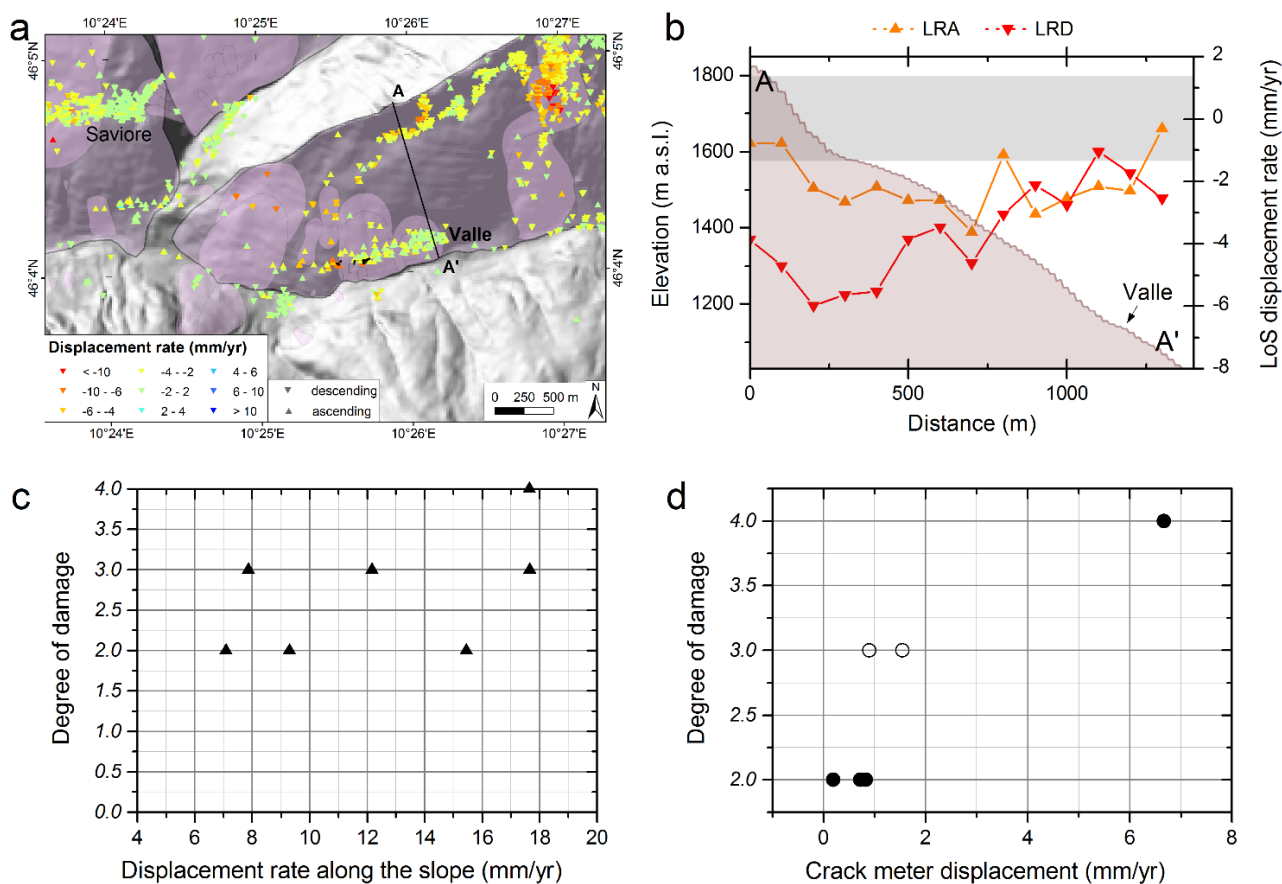


Figure 12. Comparison between PSInSAR™ LOS displacement rate (ascending) and displacement rates monitored by ground-based optical targets. Different components of optical target displacements vectors are used: (a) vertical component, (b) north component, (c) west component, (d) composed vertical and west component, (e) composed vertical and north component and (f) total vector. The best-fitting line in panel (d) was obtained by least square regression.

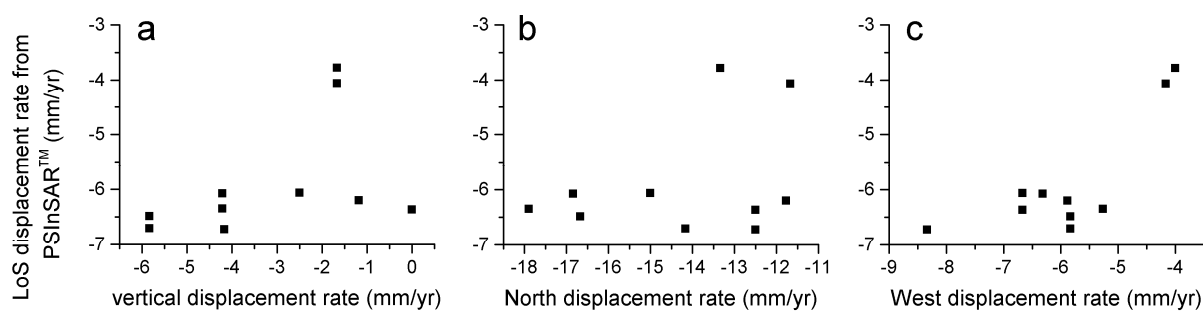
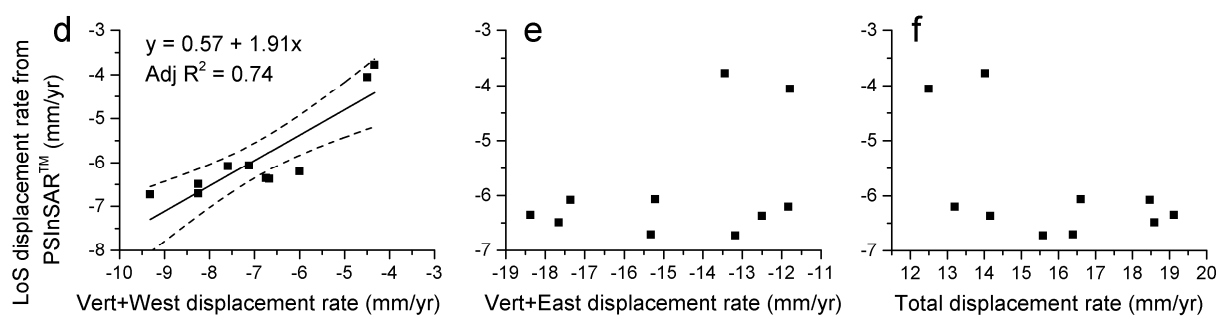


Figure 12. Cont.



Damages to buildings are heavy in the western sector of the village, where buildings have been surveyed, and a very slight trend of increasing damage with displacement rate is observable. The rate of crack formation on the buildings, as monitored by crackmeters, has the same order of magnitude of observed PSInSAR™ displacements and shows a good correlation with the estimated degree of damage.

4.5. Catasco and Montalto Rockslides

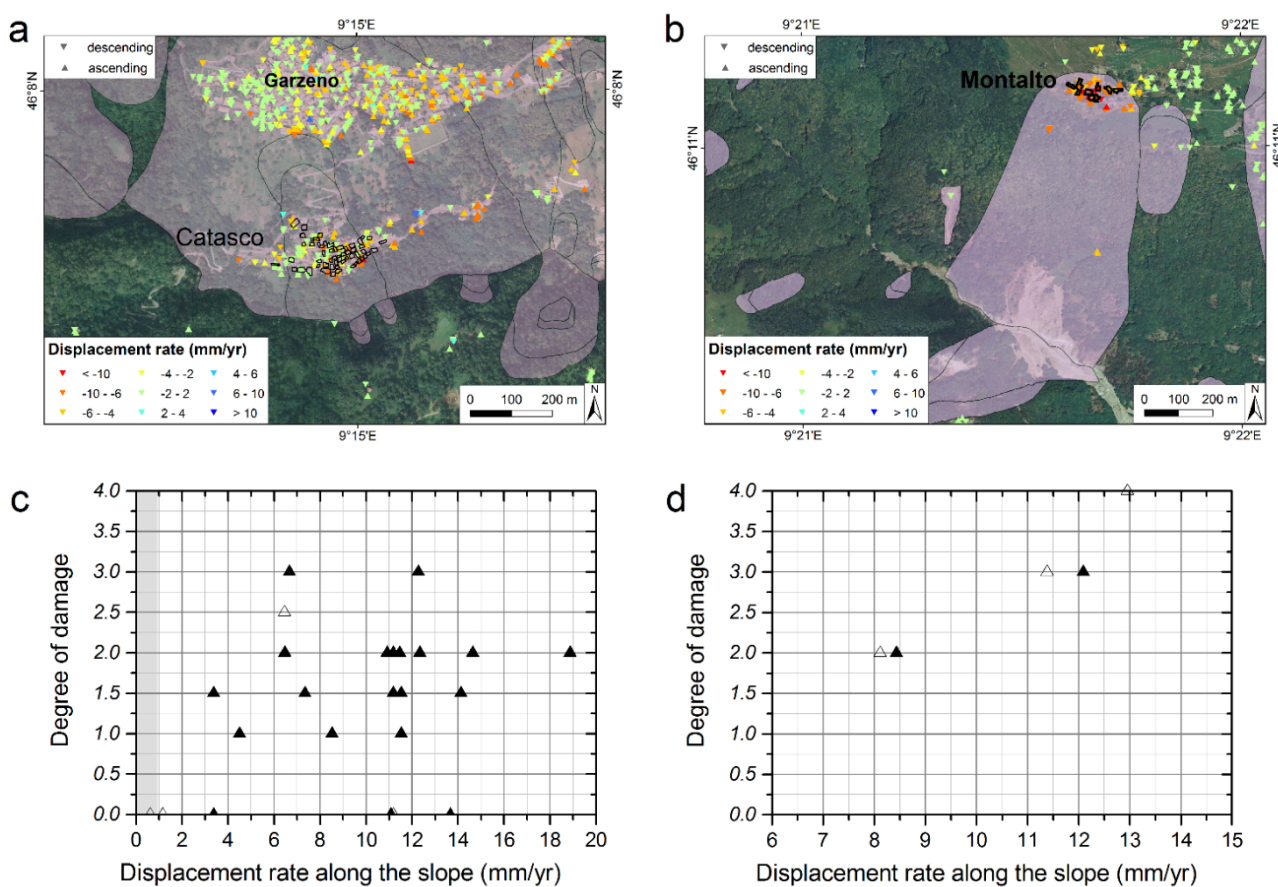
Catasco and Montalto landslides are smaller phenomena not classified as DSGSD (Figure 13). The instability that affects Catasco village (Figure 13a,c) is characterized by a large rockslide, which is partially active, with movements mostly localized in the eastern part of the village [55]. Notwithstanding the presence of long-term damage, the landslide complex has been only recently identified and mapped, and it was not studied systematically.

Only in 2010 was on-site monitoring activity started in the Catasco village. The lower part of the village is characterized by a relatively shallow landslide (about 5 m deep) affecting the colluvial soil cover, while the upper part lies within a 30 m-deep rotational rockslide, as witnessed by inclinometer measurements available since 2010. The complex landslide behavior causes differential movements at the surface. These generate moderate-to-heavy damage to buildings, the latter related to buildings located in the lower part of the village, where the effect of shallow landsliding has been stronger.

The correlation between the degree of damage and the displacement rate is poor, probably due to the orientation of the slope, which is not optimal for the radar technique, and to the existence of different phenomena resulting in different deformations.

Montalto village (Figure 13b,d) lies at the head of a large rockslide, part of which has been very active since 1998, with a strong acceleration in 2002. The upper sector of the landslide shows a significant displacement in both ascending and descending modes (Figure 13b). Considering that the rockslide faces south, we can interpret the measured displacement as the vertical component of the movement associated with the landslide head. A possible horizontal component is not resolved by the satellites, but can be assumed as almost negligible with respect to the vertical component, due to the high slope gradient and the shape of the landslide. Damage to surveyed buildings is heavy, with a strong correlation between the degree of damage and the displacement rate (Figure 13d).

Figure 13. Displacement rate and damage to buildings for the Catasco and Montalto rockslides. (a) PSInSAR™ displacement rate map and location of the surveyed buildings for the Catasco rockslide (black polygons); (b) PSInSAR™ displacement rate map and location of the surveyed buildings for the Montalto rockslide (black polygons); (c) damage degree of buildings of the Catasco rockslide as a function of the displacement rate for the LRA dataset; (d) damage degree of buildings of the Montalto rockslide as a function of the displacement rate for the LRA dataset. Solid and open triangles in panels (c,d) refer to buildings with and without wall coating, respectively. The grey area in panel (c) represents the average standard deviation (Table 2).



5. Discussion

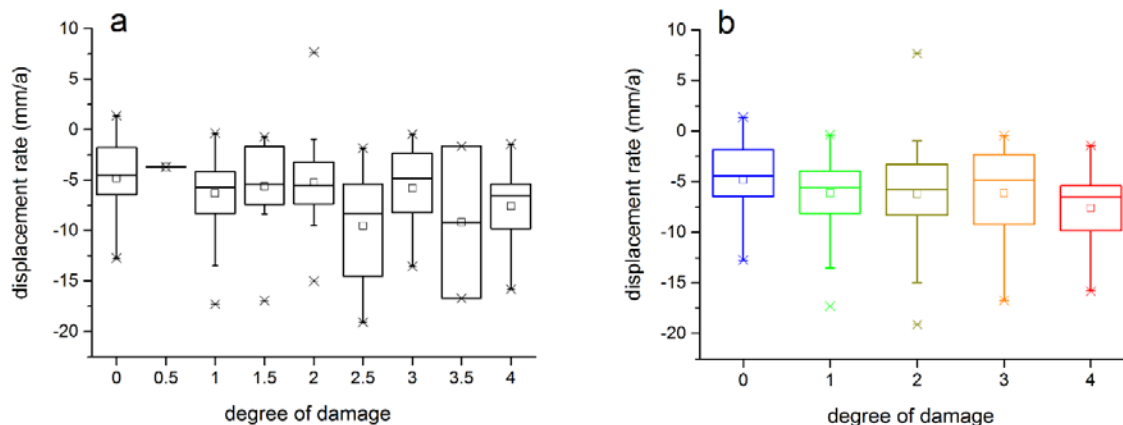
The PSInSAR™ technique provides useful information for the analysis of DSGSDs and large rockslide characterized by low displacement rates. We showed in the analysis of the studied sites that PSInSAR™ could be used to describe the activity of slope instabilities and, also, the behavior and kinematics of the landslides. For instance, a progressive decrease of the displacement rate downslope could indicate a circular or compound failure mechanism. This analysis could benefit from the reconstruction of the actual displacement vector, at least in the E-W direction, by combining ascending- and descending-mode data [30,49]. Even if this reconstruction was not possible for all the studied sites, because of the scarcity of couples of ascending and descending data for the same points in space, we have shown the importance of considering both acquisition modes, especially for the example of Lake Palù DSGSD.

The PSInSARTM data seems also suitable for the analysis of displacement rates associated with the damage of structures and infrastructures. Although this correlation is not always clear for the studied sites, the general trend of the data observed in box and whiskers plots (Figure 14) shows that the degree of damage is significantly correlated with the displacement rate. For instance, considering the 25th-percentile of the displacement rate (Figure 14b), we observe that this varies linearly between -5 and -10 mm/yr from a damage level of 0 to a damage level of 4. The distributions of the displacement rate values for each degree of damage (Figure 14) are very dispersed, due to a large uncertainty. This uncertainty mainly derives from the complexity of the slope instability behavior, sometimes from the difficulty of associating a unique damage value to a structure, and, finally, the different position of the structure within the landslide.

The best correlation between the degree of damage and the displacement rate is observed for the Montalto rockslide. Although the number of surveyed buildings is low, we can argue that the good correlation is due to the fact that buildings are all located in the same area of the landslide, where the behavior is homogeneous. Moreover, the Montalto rockslide is the smallest phenomenon analyzed (0.32 km^2), also showing the most simple kinematic behavior, which consists in the rotation of the whole slide mass.

The Mt. Legnoncino DSGSD also shows a good correlation between the degree of damage and the displacement rate, although some buildings show an anomalous degree of damage. In particular, a few buildings have a small degree of damage notwithstanding a large displacement rate. These buildings present recent wall coatings, possibly covering minor damages to the structure. This problem has been observed also at other sites, where walls of many buildings appeared to have been recently repaired and rendered. In those cases, the estimated degree of damage can be strongly underestimated. It must be stressed that some buildings have been built using different techniques and materials and at very different times. This can control the level of damage. Furthermore, in the case of slow moving landslides, old structures could have been subjected to a larger cumulated displacement or more acceleration events.

Figure 14. Box and whiskers plots of all displacement rate values for each degree of damage for all surveyed buildings at all the seven sites. (a) The original degree of damage values considering half degree intervals; (b) truncated values of the degree of damage. Box: 25th-, 50th- and 75th-percentile; whiskers: fifth- and 95th-percentile; square: mean.



For the Lake Palù and Mt. Padrio-Varadega DSGSDs, we observe a poor correlation between the degree of damage and the displacement rate. Here, the surveyed buildings are widespread over the DSGSD, thus belonging to different sectors with different displacement rates and behavior. These buildings are subjected to a different style of movement (e.g., dominant vertical vs. horizontal movement), which induces different effects on the buildings and a different degree of damage.

For larger DSGSDs (Mt. Padrio-Varadega, Caspoggio and Legnoncino) with very deep failure surfaces, it is also likely that the movement of the phenomenon occurs without large ground surface differential movements, except along some specific morpho-structures, which can actually cause damage to building foundations and structures [26]. In this case, the movement of the structure can occur as a slight rigid translation of the structure, without any evident damage.

Finally, for the Saviore DSGSD and Catasco rockslide, the poor correlation between the degree of damage and the displacement rate can be attributed to the low capability of the PSInSAR™ technique to detect movements mainly directed toward north or south, thus parallel to the satellite orbit and perpendicular to the LOS.

6. Conclusion

PSInSAR™ displacement data have been used for the analysis of deep-seated gravitational slope deformations (DSGSD) and large rockslide activity and kinematics in Alpine terrains. The main aim of the analysis was to investigate the correlation between the displacement rate and the degree of damage of buildings. In fact, no real effort has been done in the literature to verify the use of PSInSAR™ for building damage assessment and monitoring. The analysis of displacement data shows a continuous slope movement of DSGSD and rockslides with the presence of diffuse deformation along the slope. Displacement rates up to 20 mm/yr were calculated along the slope direction at most of the sites. In general, we observe an increase of the degree of damage when the displacement rate increases. For instance, the 25th-percentile of the measured displacement rates has been observed to increase linearly between -5 and -10 mm/yr for a damage level varying from null (damage level = 0) to very heavy (damage level = 4) (Figure 14b). However, this trend shows a large uncertainty, which can be due to different causes, such as:

- the uncertainty in the attribution of the degree of damage to recently renovated buildings;
- the complexity of the deformation for large phenomena, with differential behavior within the slope instability, due to reactivation of smaller events, which can locally increase the observed degree of damage, or the presence of debris at the surface;
- the possible absence of differential superficial movements causing damages to structures, due to the large size of the investigated phenomena; and
- the different behavior of buildings, depending on the type of structure, its age, the position along the slope and the occurrence of total/local recent reactivation/accelerations.

Future improvements of the PSI techniques could provide benefits to the analysis of large rock instabilities, especially due to the reduction of revisiting time and the improvement of resolution offered by other satellites (e.g., Cosmo SkyMed, TerraSAR-X, Sentinel). These developments will permit one to better define the instability behavior, to increase the PS density and the size of the

structures database and to improve the possibility of reconstructing the actual displacement vector by combining ascending and descending data, referring to corresponding spatial positions.

Acknowledgments

We thank A. Ferretti from Tele-Rilevamento Europa and M. Ceriani from Regione Lombardia for making PSInSAR™ data available. The building damage survey was actively performed by E. D'Agostini and, for the Valle di Savio, by M. Salvoni. The extraction of displacement swath profile was done by R. Ignagnaro.

Conflict of Interest

The authors declare no conflict of interest.

References and Notes

1. Ambrosi, C.; Crosta, G.B. Large sackung along major tectonic features in the Central Alps. *Eng. Geol.* **2006**, *83*, 183–200.
2. MacFarlane, D.F. Observations and predictions of the behaviour of large, slow-moving landslides in schist, Clyde Dam reservoir, New Zealand. *Eng. Geol.* **2008**, *109*, 5–15.
3. Zangerl, C.; Eberhardt, E.; Perzmaier, S. Kinematic behaviour and velocity characteristics of a complex deep-seated crystalline rockslide system in relation to its interaction with a dam reservoir. *Eng. Geol.* **2010**, *112*, 53–67.
4. Cruden, D.M.; Varnes, D.J. Landslide Types and Processes. In *Landslides: Investigation and Mitigation*; Turner, A.K., Shuster, R.L., Eds.; Transportation Research Board: Washington, DC, USA, 1996; pp. 36–75.
5. Crosta G.B.; Agliardi, F.; Frattini, P. Deep seated gravitational slope deformations in the European Alps. *Tectonophysics* **2013**, *605*, 13–33.
6. Zischinsky, U. On the Deformation of High Slopes. In Proceedings of 1st Congress International Society for Rock Mechanics 2, Lisbon, Portugal, 25 September–1 October 1966; pp. 179–185.
7. Bovis, M.J. Rock-slope deformation at Affliction Creek, southern Coast Mountains, British Columbia. *Geol. Soc. Am. Bull.* **1990**, *93*, 804–812.
8. Varnes, D.J.; Radbruch-Hall, D.; Varnes, K.L.; Smith, W.K.; Savage W.Z. *Measurement of Ridge-Spreading Movements (Sackungen) at Bald Eagle Mountain, Lake County, Colorado, 1975–1989*; US Geological Survey Open-File Report 90-543; US Geological Survey: Denver, CO, USA, 1990; p. 13.
9. Chigira, M. Long-term gravitational deformation of rock by mass rock creep. *Eng. Geol.* **1992**, *32*, 157–184.
10. Agliardi, F.; Crosta, G.; Zanchi, A. Structural constraints on deep-seated slope deformation kinematics. *Eng. Geol.* **2001**, *59*, 83–102.
11. Cruden, D.M.; Hu, X.Q. Exhaustion and steady-state models for predicting landslide hazards in the Canadian Rocky Mountains. *Geomorphology* **1993**, *8*, 279–285.

12. Hippolyte, J.-C.; Brocard, G.; Tardy, M.; Nicoud, G.; Boulès, D.; Braucher, R.; Ménard, G.; Souffaché, B. The recent fault scarps of the Western Alps (France): Tectonic surface ruptures or gravitational sacking scarps? A combined mapping, geomorphic, levelling, and ^{10}Be dating approach. *Tectonophysics* **2006**, *418*, 255–276.
13. Hippolyte, J.C.; Boulès, D.; Braucher, R.; Carcaillet, J.; Léanni, L.; Arnold, M.; Aumaitre, G. Cosmogenic ^{10}Be dating of a sacking and its faulted rock glaciers, in the Alps of Savoy (France). *Geomorphology* **2009**, *108*, 312–320.
14. Bigot-Cormier, F.; Braucher, R.; Boulès, D.; Guglielmi, Y.; Dubar, M.; Stéphan, J.F. Chronological constraints on processes leading to large active landslides. *Earth. Planet. Sci. Lett.* **2005**, *235*, 141–150.
15. Bovis, M.J.; Evans, S.G. Extensive deformations of rock slopes in southern Coast Mountains, southwest British Columbia, Canada. *Eng. Geol.* **1996**, *44*, 163–182.
16. Curlander J.C.; McDonough R.N. *Synthetic Aperture Radar Systems and Signal Processing*; Wiley-Interscience: New York, NY, USA, 1991.
17. Ferretti, A.; Prati, C.; Rocca, F. Multibaseline InSAR DEM reconstruction: The wavelet approach. *IEEE Trans. Geosci. Remote Sens.* **1999**, *37*, 705–715.
18. Ferretti, A.; Prati, C.; Rocca, F. Nonlinear subsidence rate estimation using permanent scatterers in differential SAR interferometry. *IEEE Trans. Geosci. Remote Sens.* **2000**, *38*, 2202–2212.
19. Ferretti, A.; Prati, C.; Rocca, F. Multibaseline phase unwrapping for InSAR topography estimation. *Nuovo Cimento Della Soc. Ital. Fis. C* **2001**, *124*, 159–176.
20. Ferretti, A.; Prati, C.; Rocca, F. Permanent scatterers in SAR Interferometry. *IEEE Trans. Geosci. Remote Sens.* **2001**, *39*, 8–20.
21. Allievi, J.; Ambrosi, C.; Ceriani, M.; Colesanti, C.; Crosta, G.B.; Ferretti, A.; Fossati, D. Monitoring Slow Mass Movements with the Permanent Scatterers technique. In Proceedings of the IEEE International Geoscience and Remote Sensing Symposium (IGARSS'03), Toulouse, France, 21–25 July 2003; Volume 1, pp. 215–217.
22. Colesanti, C.; Crosta, G.B.; Ferretti, A.; Ambrosi, C. Monitoring and assessing the state of activity of slope instabilities by the Permanent Scatterers Technique. *NATO Sci. Ser.* **2006**, *49*, 175–194.
23. Saroli, M.; Stramondo, S.; Moro, M.; Doumaz, F. Movements detection of deep seated gravitational slope deformations by means of InSAR data and photogeological interpretation: northern Sicily case study. *Terra Nova* **2005**, *17*, 35–43.
24. Strozzi, T.; Farina, P.; Corsini, A.; Ambrosi, C.; Thüning, M.; Zilger, J.; Wiesmann, A.; Wegmüller, U.; Werner, C. Survey and monitoring of landslide displacements by means of L-band satellite SAR interferometry. *Landslides* **1995**, *2*, 193–201.
25. Colesanti, C.; Wasowski, J. Investigating landslides with space-borne Synthetic Aperture Radar (SAR) interferometry. *Eng. Geol.* **2006**, *88*, 173–199.
26. Osmundsen, P.T.; Henderson, I.; Lauknes, T.R.; Larsen, Y.; Redfield, T.F.; Dehls, J. Active normal fault control on landscape and rock-slope failure in northern Norway. *Geology* **2006**, *37*, 135–138.

27. Strozzi, T.; Delaloye, R.; Käab, A.; Ambrosi, C.; Perruchoud, E.; Wegmüller, U. Combined observations of rock mass movements using satellite SAR interferometry, differential GPS, airborne digital photogrammetry, and airborne photography interpretation. *J. Geophys. Res.* **2010**, *115*, F01014.
28. Calò, F.; Calcaterra, D.; Iodice, A.; Parise, M.; Ramondini, M. Assessing the activity of a large landslide in southern Italy by ground-monitoring and SAR interferometric techniques. *Int. J. Remote Sens.* **2012**, *33*, 3512–3530.
29. Del Ventisette, C.; Ciampalini, A.; Manunta, M.; Calò, F.; Paglia, L.; Ardizzone, F.; Mondini, A.; Reichenbach, P.; Mateos, R.M.; Bianchini, S.; *et al.* Exploitation of large archives of ERS and ENVISAT C-band SAR data to characterize ground deformations. *Remote Sens.* **2013**, *5*, 3896–3917.
30. Tofani, T.; Raspini, F.; Catani, F.; Casagli, N. Persistent Scatterer Interferometry (PSI) technique for landslide characterization and monitoring. *Remote Sens.* **2013**, *5*, 1045–1065.
31. Strozzi, T.; Ambrosi, C.; Raetzo, H. Interpretation of aerial photographs and satellite SAR interferometry for the inventory of landslides. *Remote Sens.* **2013**, *5*, 2554–2570
32. Tarchi, D.; Casagli, N.; Leva, D.; Moretti, S.; Sieber, A.J. Monitoring landslide displacements by using ground-based SAR interferometry: Application to the Ruinon landslide in the Italian Alps. *J. Geophys. Res.* **2003**, *108*, 2387–2401.
33. Moore D.P.; Watson, A.D.; Martin, C.D. Deformation Mechanism of a Large Rockslide Inundated by a Reservoir. In Proceedings of JTC Workshop on the Mechanics and Velocity of Large Landslides, Courmayeur, Italy, 25–28 September 2006.
34. Negulescu, C.; Foerster, E. Parametric studies and quantitative assessment of the vulnerability of a RC frame building exposed to differential settlements. *Nat. Hazard. Earth Syst. Sci.* **2010**, *10*, 1781–1792.
35. Mansour, M.F.; Morgenstern, N.R.; Martin, C.D. Expected damage from displacement of slow-moving slides. *Landslides* **2010**, *8*, 117–131.
36. Fotopoulou, S.; Ptilakis, K. Vulnerability assessment of reinforced concrete buildings subjected to seismically triggered slow-moving earth slides. *Landslides* **2012**, doi: 10.1007/s10346-012-0345-5.
37. Crosta, G.B.; Agliardi, F.; Frattini, P.; Zanchi, A. Alpine inventory of Deep-Seated Gravitational Slope Deformations. *Geophys. Res. Abstr.* **2008**, *10*, EGU2008-A-02709.
38. Agliardi, F.; Crosta, G.B.; Frattini, P. Slow Rock-Slope Deformation. In *Landslides: Types, Mechanisms and Modeling*; Clague, J.J., Stead, D., Eds.; Cambridge University Press: Cambridge, UK, 2012; pp. 207–221.
39. Agliardi, F.; Crosta, G.B.; Frattini, P.; Malusà, M. Giant non-catastrophic landslides and the long-term exhumation of the European Alps. *Earth. Planet. Sci. Lett.* **2013**, *365*, 263–274.
40. Schmid, S.M.; Fogenschuh, B.; Kissling, E.; Schuster, R. Tectonic map and overall architecture of the Alpine orogen. *Eclogae Geol. Helv.* **2004**, *97*, 93–117.
41. Schönborn, G. Alpine tectonics and kinematic models of the central Southern Alps. *Mem. Sci. Geol.* **1992**, *44*, 229–393.
42. Froitzheim, N.; Schmid, S.M.; Conti, P. Repeated change from crustal shortening to orogen-parallel extension in the Austroalpine units of Graubünden. *Eclogae Geol. Helv.* **1994**, *87*, 559–612.

43. *Geologische Karte der Schweiz 1:500,000*; Institut für Geologie, Universität Bern, und Bundesamt für Wasser und Geologie: Bern, Switzerland, 2005.
44. Refice, A.; Bovenga, F.; Guerriero, L.; Wasowski, J. DInSAR Applications to Landslide Studies, In Proceedings of the IEEE International Geoscience and Remote Sensing Symposium (IGARSS'01), Sydney, Australia, 9–13 July 2001; Volume 1, pp. 144–146.
45. Werner, C.; Wegmuller, U.; Strozzi, T.; Wiesmann, A. Interferometric Point Target Analysis for Deformation Mapping. In Proceedings of the IEEE International Geoscience and Remote Sensing Symposium (IGARSS'03), Toulouse, France, 21–25 July 2003; Volume 7, pp. 4362–4364.
46. Hooper, A.; Zebker, H.; Segall, P.; Kampes, B. A new method for measuring deformation on Volcanoes and other natural terrains using InSAR persistent scatterers. *Geophys. Res. Lett.* **2004**, *31*, L23611.
47. Bovenga, F.; Nutricato, R.; Refice, A.; Wasowski, J. Application of multi-temporal differential interferometry to slope instability detection in urban/peri-urban Areas. *Eng. Geol.* **2006**, *88*, 218–239.
48. Colesanti, C.; Ferretti, A.; Locatelli, R.; Novali, F.; Savio, G. Permanent Scatterers: Precision Assessment and Multi-Platform Analysis. In Proceedings of IEEE Geoscience and Remote Sensing Symposium (IGARSS'03), Toulouse, France, 21–25 July 2003; pp. 1193–1195.
49. Cascini, L.; Fornaro, G.; Peduto, D. Advanced low- and full-resolution DInSAR map generation for slow-moving landslide analysis at different scales. *Eng. Geol.* **2010**, *112*, 29–42.
50. Cigna, F.; Bianchini, S.; Casagli, N. How to assess landslide activity and intensity with Persistent Scatterer Interferometry (PSI): the PSI-based matrix approach. *Landslides* **2012**, *5*, 1–17.
51. Grunthal, G. *European Macroseismic Scale EMS-98*; Conseil de l'Europe, Cahiers du Centre Européen de Géodynamique et de Seismologie: Luxembourg, 1998; Volume 15, p. 101. Available online: <http://www.gfz-potsdam.de/en/research/organizational-units/departments-of-the-gfz/departement-2/seismic-hazard-and-stress-field/products-and-services/ems-98/> (accessed on 24 September 2013).
52. Cossa, A. Analisi Dell'Evoluzione e Modellazione di Fenomeni di Instabilità di Versante Presso L'Impianto Idroelettrico di Lanzada (Valmalenco, SO). M.Sc. Thesis, University of Milano-Bicocca, Milan, Italy, 2006.
53. Istituto Sperimentale Modelli e Strutture (ISMES). *Studio per la Definizione dei Livelli di Soglia e Delle Procedure di Analisi dei Dati Strumentali Della Rete di Monitoraggio di Savio dell'Adamello (BS)*; Technical Report No. 1; ISMES: Bergamo, Italy, 1999; unpublished.
54. Salvoni, M. Censimento e Monitoraggio Delle Lesioni Strutturali ed Analisi del Dissesto di Valle di Savio ai Fini di Una Valutazione Quantitativa del Rischio. Bachelor's Thesis, University of Milano-Bicocca, Milan, Italy, 2007.
55. Nitti, D.O.; Bovenga, F.; Nutricato, R.; Rana, F.; D'Aprile, C.; Frattini, P.; Crosta, G.B.; Chiaradia, M.T.; Ober, G.; Candela, L. C- and X-band Multi-pass InSAR analysis over alpine areas (ITALY). *Proc. SPIE* **2010**, doi: 10.1117/12.849210.